

Mutual inelastic excitation in the $^{28}\text{Si} + ^{28}\text{Si}$ reaction at 19.7 and 30 MeV/nucleon

P. Decowski

*Department of Physics, Smith College, Northampton, Massachusetts 01063
and R.J. van de Graaff Laboratorium, Rijksuniversiteit te Utrecht, 3508 TA Utrecht, The Netherlands*

E. Gierlik,* P. F. Box,[†] K. A. Griffioen[‡] R. J. Meijer[§] G. J. van Nieuwenhuizen,
and R. Kamermans
R.J. van de Graaff Laboratorium, Rijksuniversiteit te Utrecht, 3508 TA Utrecht, The Netherlands

H. W. Wilschut
Kernfysisch Versneller Instituut, Zernikelaan 25, 9747 AA Groningen, The Netherlands

A. Giorni and C. Morand
Institut des Sciences Nucléaires, Avenue des Martyrs 53, F-38026 Grenoble CEDEX, France

A. Demeyer and D. Guinet
Institut de Physique Nucléaire, 43 Boulevard du 11 Novembre 1918, F-69622 Villeurbanne Cedex, France
(Received 13 December 1991)

Velocity spectra of heavy ions produced in the $^{28}\text{Si} + ^{28}\text{Si}$ reaction at 19.7 and 30 MeV/nucleon were measured and interpreted within the Q -optimum model. An important process at forward angles is the mutual excitation of projectile and target to energies localized in the region of $(2-3)\hbar\omega$ excitations.

PACS number(s): 25.70.Lm

I. INTRODUCTION

The complex dynamics of heavy ion interactions at bombarding energies well above the Coulomb barrier still requires a large experimental effort for full clarification. Properties of hot and compressed nuclei formed in collisions at small impact parameters are now in the focus of experimental investigations. More peripheral collisions, essentially binary, reveal a rich variety of processes ranging from quasielastic to deeply inelastic interactions accompanied by extensive exchange of nuclear matter. At impact parameters somewhat larger than the sum of the nuclear radii the Coulomb potential induces single-phonon and multiphonon excitations of low-energy states in the reaction partners. For grazing collisions the nuclear potential is able to excite phonon modes at much higher frequencies (giant resonances) [1-3]. This mechanism, selective in the initial excitation energy, may contribute substantially to the energy dissipation process in a heavy ion reaction.

This paper concentrates on an experimental investigation of peripheral interactions of silicon nuclei at bombarding energies of a few tens MeV/nucleon. The focus of our study was a mutual inelastic excitation of both reaction partners which, as we found, is a dominant process at forward angles. The choice of a reaction such as $^{28}\text{Si} + ^{28}\text{Si}$, with identical projectile and target, simplifies the data analysis due to the fore-aft symmetry of all processes in the center-of-mass (c.m.) frame. This symmetry also plays an important role in the interpretation of the results. The experimental setup is described in Sec. II; Sec. III presents experimental results discussed in Sec. IV. Section V examines the probability of mutual excitation; conclusions are given in Sec. VI.

II. EXPERIMENT

A Si target ($370 \mu\text{g}/\text{cm}^2$ thick) was bombarded by ^{28}Si projectiles accelerated to energies of 19.7 and 30 MeV/nucleon by the SARA facility (Grenoble). Heavy residues (HR's) of the reaction were detected in a small ionization chamber-Si detector telescope ($\Delta\Omega = 0.8 \text{ msr}$) which was placed at forward angles ($3^\circ, 5^\circ, 7^\circ, 11^\circ, 13^\circ, 18^\circ, 23^\circ$ at 19.7 MeV/nucleon and $3^\circ, 4^\circ, 6^\circ, 8^\circ, 10^\circ, 12^\circ, 16^\circ, 20^\circ$ at 30 MeV/nucleon). The HR telescope provided the energy and element number of all observed residues with $Z \geq 6$ and $Z \geq 8$ at incident energies of 19.7 and 30 MeV/nucleon, respectively (the cut at low Z values eliminates ions not stopped by the 1 mm thick Si detector in back of the ionization chamber). The tar-

*On leave from the Institute of Experimental Physics, University of Warsaw, Poland.

[†]Present address: IPN, Orsay, France.

[‡]Present address: University of Pennsylvania, Philadelphia, PA 19104.

[§]Present address: PTT Research, Groningen, The Netherlands.

get was surrounded by 16 Si-CsI light-particle telescopes from the Utrecht multidetector system [4, 5] placed both in-plane and out-of-plane. The possibility of rotating the system allowed us to measure coincidences between heavy residues and light particles at 32 angles distributed over a large part of the total solid angle. In the coincidence measurements the HR telescope was placed at each of the two most forward angles (4° and 6° at 19.7 MeV/nucleon, 3° and 6° at 30 MeV/nucleon) where the yield of the HR's was the largest. Full experimental details can be found in Ref. [6].

III. RESULTS

HR velocity spectra were constructed using the energy and charge deduced from the HR telescope and the average mass deduced from the charge-mass relation along the line of beta stability. Examples of these spectra are shown in Fig. 1. The evaporation residue (ER) peak, centered at half of the beam velocity, is pronounced in the spectra of residues with $Z > 15$. Spectra of lighter residues are dominated by more peripheral processes, characterized by velocities close to the beam velocity (6.1 and 7.6 cm/ns at incident energies of 19.7 and 30 MeV/nucleon, respectively).

Taking the reflection symmetry with respect to the velocity of the center of mass $V_{c.m.}$ into account, the HR velocity spectra were described by a set of functions, which have the form

$$F_{n_0, x_0, \sigma}(x) = x^2 \left(\sqrt{2\pi x_0} \frac{x_0^x}{\Gamma(x+1)} e^{-x_0} \right)^{x_0/\sigma^2}, \quad (1)$$

where x is the channel number in a spectrum counted from an initial channel n_0 , and x_0 has a value between 0 and a channel number corresponding to the velocity $V_{c.m.}$. For large x_0 , $F_{n_0, x_0, \sigma}(x)$ becomes the Maxwellian distribution $x^2 e^{-(x-x_0)^2/2\sigma^2}$. In analogy to the Poisson distribution, for small x_0 , Eq. (1) possesses the skewness needed to describe the phase-space limitations at velocities close to the beam or target velocities. It can be seen in Fig. 1 that with a limited number (≤ 7) of $F_{n_0, v_0, \sigma}$'s it was possible to obtain a good description ($\chi^2 < 2$) of the experimental velocity spectra for all measured HR's. This parametrization allowed us to construct contour lines of the invariant cross section in the velocity versus Z plane. The velocities between discrete Z values in the (Z, v) plane were calculated using a linear interpolation of parameters from the neighboring spectra. Transition to a continuous Z variable facilitated not only drawing smooth contour plots of the experimental cross sections, but also enabled creating spectra along arbitrary cuts in the v versus Z plane which appeared to be useful in the further analysis of the data. However, one has to be aware of the fact that without a proper normalization this procedure induces an artificial excess of the cross section in the regions between the discrete Z values. Any integration of the cross section along these cuts yields an overestimated value.

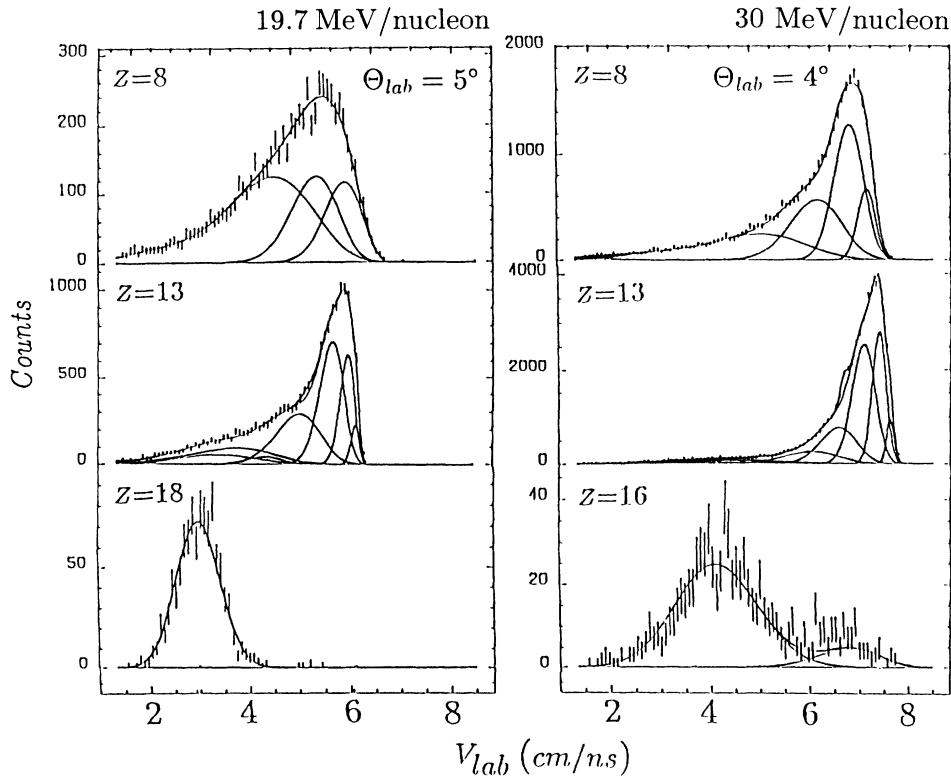


FIG. 1. Examples of heavy residue velocity spectra at incident energies of 19.7 and 30 MeV/nucleon. The solid lines show the Maxwellian-like functions used to describe the spectra.

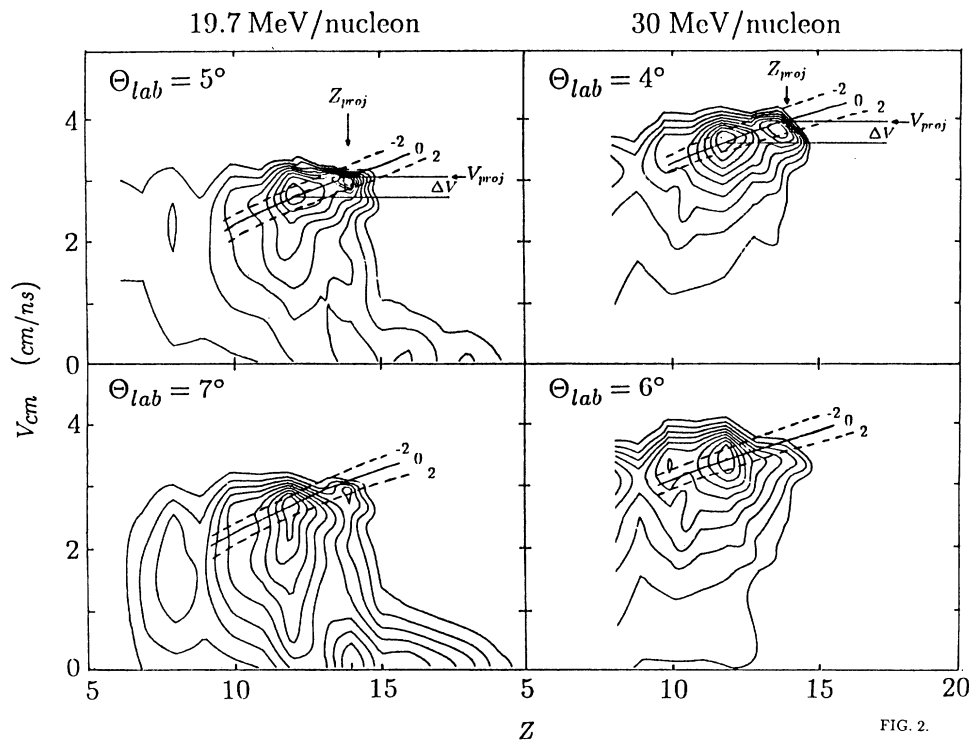


FIG. 2. Contour plots of the experimental invariant cross sections in the Z_{residual} versus $v_{\text{c.m.}}$ plane. The solid and dashed lines show the Q -optimum model calculations for net transfers of 0 and ± 2 nucleons, respectively.

Examples of contour plots are shown in Fig. 2. The fitted component corresponding to the strong elastic peak was deliberately removed from the plots. The contour lines are drawn in steps of 10% of the maximum cross section.

The pattern of contour lines indicates that at both bombarding energies a dominant process occurs, which is characterized by a concentration of the cross section at velocities smaller by $\Delta v = 0.33 \pm 0.05$ cm/n.s than the projectile velocity (see Fig. 2). The origin of this maximum cannot be an impurity in the target. The only possible reaction that produces evaporation residues at such high velocities is a reaction with hydrogen. This possibility can be easily ruled out on the basis of the Δv value which is twice that expected from $^{28}\text{Si} + ^1\text{H}$. Several other arguments reinforce this: (1) The most likely Z lies near $Z = 12$, whereas statistical-model calculations for Si+H show that mainly $Z = 13$ would be populated. (2) Reactions on a hydrogen impurity would be kinematically focused within 3° , and this is not the case for the data. (3) The intensity of the source in the data is far larger than is possible for an impurity. In the test run at the Utrecht Van de Graaff accelerator, elastic scattering of α particles and ^{12}C from the Si targets after the experiment showed that C and O are the primary contaminants, and together they contribute less than 10% to the total number of atoms in the target.

If one assumes that, at velocities and Z values close to those of the incident projectile, binary peripheral reactions dominate, then any excitation of the projectile must, as a consequence of the symmetry of our system, have its counterpart in the excitation of the target. In the case of a selective excitation of either the projec-

tile or the target we would see two maxima in the contour plot at the same velocity: one at $Z < Z_{\text{proj}}$ (the residue of the excited projectile/target) and another one at $Z = Z_{\text{proj}} = Z_{\text{targ}}$ (the nonexcited partner). Any other selective process (involving, e.g., mass transfer) will again produce two maxima (although in this case usually at different velocities). The fact that we see only one strong maximum (the other maximum in close proximity of the projectile charge and velocity originates from low-lying inelastic reactions and cannot be a partner of the discussed process) indicates that the observed maximum is connected with *mutual* excitation of the target and projectile. In such a case the value Δv determines uniquely the favorable excitation energy of both reaction partners. It turns out to be 34 ± 5 MeV at both bombarding energies.

IV. ANALYSIS AND THE DISCUSSION

A. Q -optimum model

To obtain a more quantitative description of the results, the data were analyzed within the Q -optimum model [7], extended by the inclusion of the cooling of excited fragments by particle evaporation. This model uses a "participant-spectator" scenario in which the Q value of a reaction is determined by the cluster transfer of n nucleons from the projectile a to the target A and of m nucleons from the target to the projectile: $b = a - n + m$ and $B = A - m + n$:

$$Q = U_f - U_i - (E_i - U_i) \sin^2 \beta, \quad (2)$$

with

$$\cos^2 \beta = \frac{\mu_{Aa}}{\mu_{Bb}} \left(1 - \frac{n}{a} - \frac{m}{A} \right)^2. \quad (3)$$

The Coulomb potentials U_i and U_f in the entrance and exit channels are calculated at the point of contact, E_i is the c.m. kinetic energy in the entrance channel and μ_{Aa} and μ_{Bb} are the reduced masses in the entrance and exit channels, respectively. The net mass transfer is $|n - m|$. The impact parameter and the corresponding rotational energies of both reaction partners are simply determined by the condition that the overlap of the two interacting spheres must contain $N = \max(n, m)$ nucleons. Thermal excitation energy was assumed to be shared proportionally to the number of nucleons picked up by projectile and target [8]. In our case of a symmetric system which interacts at a relatively high energy, this simple assumption might be justified because binding energy effects are averaged out and changes in the Coulomb energy are small in comparison with the total interaction energy (a discussion of these effects can be found in [9]). In the Q -optimum model scenario the damping process is due to a bidirectional flow of an equal number of nucleons. Because the model is based on pure kinematic considerations it provides a simple way to relate excitation energy and momentum transfer. However, one has to have in mind that the underlying microscopic picture of the damping process may differ from that of the nucleon exchange.

The evaporation process is taken into account in an average way based on results obtained from CASCADE [10] calculations with different heavy-ion systems. The average excitation energy per evaporated charge $\langle \epsilon \rangle$ (evaporated in the form of protons and α particles) calculated for compound systems ranging from ^{28}Si to ^{56}Ni at excitation energies between 30 and 285 MeV and spins $(0-40)\hbar$ is plotted in Fig. 3 as a function of $(E_{\text{exc}} - E_{\text{rot}})/T_0$

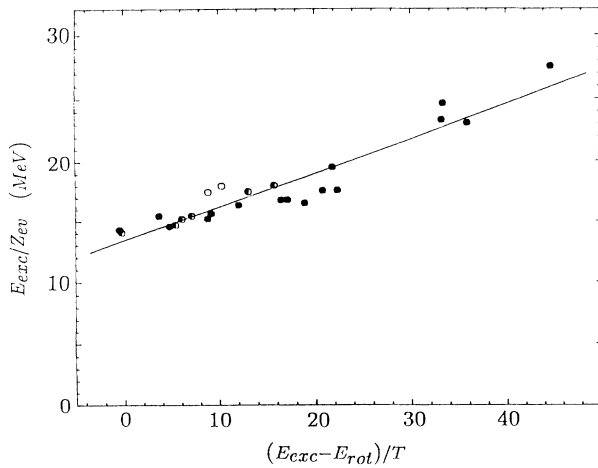


FIG. 3. Systematics of the average excitation energy removed per evaporated charge. Open, half-full, and full points show statistical model calculations for the decay of ^{28}Si , ^{40}Ca , and ^{56}Ni nuclei, respectively, at various excitation energies and spins.

(E_{ex} , E_{rot} , and $T_0 = \sqrt{8E_{\text{ex}}/A_{CN}}$ are the initial excitation energy, rotational energy and temperature of the decaying compound system with initial mass A_{CN} , respectively). The calculated values of $\langle \epsilon \rangle$ versus this coordinate exhibit a regular pattern following a line that can be parametrized by

$$\langle \epsilon \rangle = a_0 + a_1 \frac{E_{\text{ex}} - E_{\text{rot}}}{T_0}, \quad (4)$$

with $a_0 = 13.40 \pm 0.40$ MeV and $a_1 = 0.280 \pm 0.020$ MeV. This parametrization was used to calculate residual Z values of the excited fragments.

Figure 4(a) shows the HR velocities calculated using the Q -optimum model as a function of the *primary* Z value. This calculation was made for Si nuclei colliding at a laboratory energy of 19.7 MeV/nucleon. The numbers in the figure give the net mass transfer expressed in number of stripped/picked-up nucleons. The vertical lines show loci of different energy dampings at fixed net mass transfer. For each Z value the minimum velocity in this binary process is determined by the Coulomb repulsion between both reaction partners (Coulomb velocity). The evaporation of light particles distorts this diagram significantly, as can be seen in Fig. 4(b), which shows the calculated velocity as a function of the *residual* Z value. The pick-up branch (positive net mass transfer) exhibits the largest distortion because in the participant-spectator scenario the receptor gains nearly all of the excitation energy [11].

The Q -optimum model allows to reconstruct average

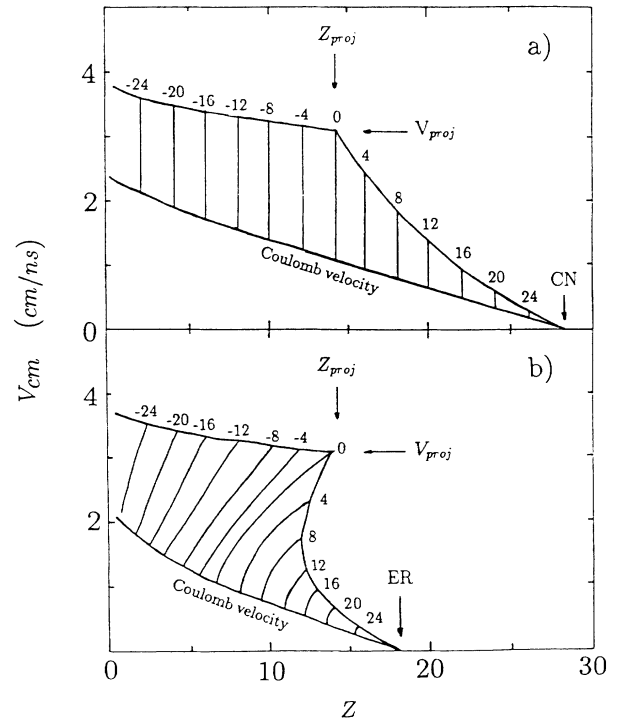


FIG. 4. Q -optimum model calculations of the heavy-residue velocity as a function of (a) the primary and (b) residual charge. The numerals indicate the net number of stripped/picked-up nucleons.

initial properties of the reaction partners after interaction (primary Z value, reaction Q value) from the velocity and Z value of the observed fragment. Although in general the applicability of this model is very limited, it is a good approximation for small net mass transfers as long as the process is binary (for zero net mass transfer—mutual excitation—the relation between the fragment average residual Z value and its average velocity v depends in a symmetric system solely on the details of the evaporation process and is independent of the interaction mechanism).

B. Q -value spectra

The line with zero net mass transfer from Fig. 4(b) (mutual inelastic scattering) is drawn on top of the contour plots in Fig. 2. At both bombarding energies the line crosses the position of the maximal cross section. This confirms the conclusion in Sec. III that the observed maximum in the HR production cross sections is due to the mutual excitation of the projectile and the target.

We have projected the cross sections from Fig. 2 within a corridor determined by the net transfer of ± 2 nucleons (to average out any fluctuations caused by the discreteness of Z values) onto the Q values calculated for each pair of v and Z values from the Q -optimum model. The results are shown in Figs. 5 and 6. At both energies, these spectra show an enhancement at Q values -60 to -80 MeV (30–40 MeV of excitation energy per partner), which is strongest at forward angles. The peak at $Z = 14$ in Fig. 2 shows up only at the most forward angles near

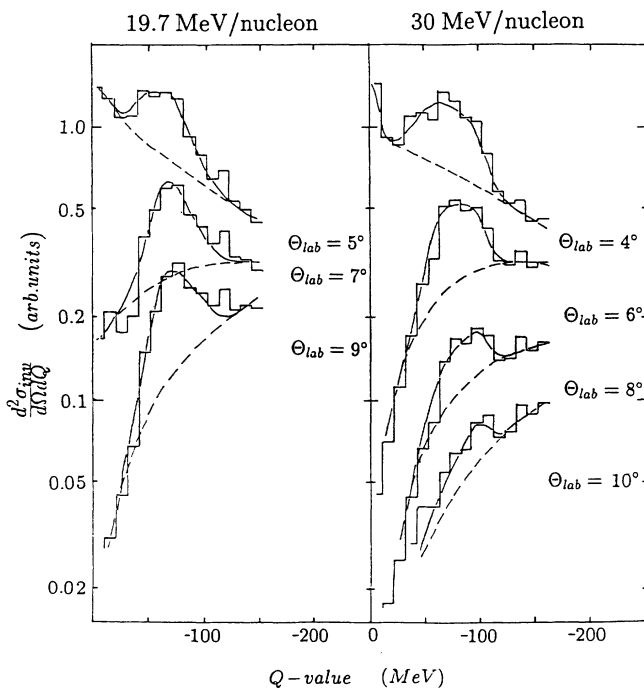


FIG. 5. Q -value spectra at various angles. The dashed and solid lines show a fitted quadratic background and a Gaussian fit to the experimental data, respectively.

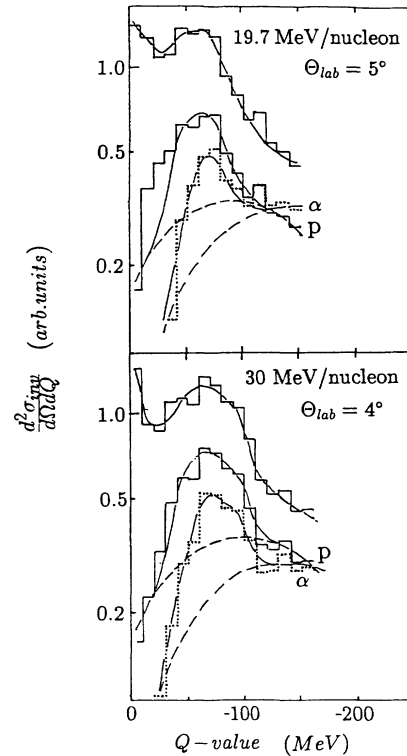


FIG. 6. Comparison between the inclusive Q -value spectra (upper solid histogram) and spectra in coincidence with emitted protons (lower solid histogram) and α 's (dotted histogram). The dashed curves show the fitted background for the coincidence data.

$Q = 0$ in Fig. 5; this is consistent with its interpretation as being due to low-energy excitations of Si below the particle-emission threshold. At larger angles deep-inelastic collisions, characterized by a large negative Q value, begin to dominate. The solid lines represent fits using Gaussian curves on top of a background described by second-order polynomials (dashed lines). All spectra in Figs. 5 and 6, representing two bombarding energies, were fit using the same three Gaussians centered at 44.7, 67.7, and 93.7 MeV with widths 9.4, 13.0, and 10.4 MeV, respectively. More than one Gaussian was needed to describe the slightly asymmetric shape of the enhancement and to account for the Q dependence of the angular distributions. At both bombarding energies the Gaussian centered at 67.7 MeV is dominant at the most forward angles.

In Fig. 6 the spectra at the smallest angles can be compared with the Q spectra obtained from contour plots of cross sections coincident with protons or α 's in any of the light particle telescopes. In this case the two coincident Q spectra are normalized arbitrarily with respect to the inclusive Q spectrum, but are properly normalized with respect to each other. They show an enhancement above the background line similar to that of the singles spectra. This indicates that the enhancement is not connected with a specific reaction channel (e.g., α transfer). The ratios of cross sections above the indicated back-

ground in the Q spectra coincident with protons and α 's (giving roughly the ratio of proton and α multiplicities) are similar at both bombarding energies: 1.60 ± 0.18 at the lower energy and 1.54 ± 0.12 at the higher energy. This is consistent with the assumption that at both energies we are dealing with approximately the same kind of projectile and target excitation.

In a dynamical scenario the selectivity of projectile and target excitations could be explained by a bidirectional nucleon transfer if the number of transferred nucleons were well correlated with the bombarding energy. Each absorbed nucleon produces an excitation energy equal to 19.7 or 30 MeV at the two bombarding energies, respectively. If one assumes that the number of transferred nucleons is proportional to the interaction time, which in turn is proportional to $1/\sqrt{E_{\text{beam}}}$, one gets a rather weak dependence of the resulting excitation on the bombarding energy: $E_{\text{ex}} \sim \sqrt{E_{\text{beam}}}$. In Fig. 7 the enhancements above background in the Q spectra are shown in more detail (linear scale). The data at 19.7 and 30 MeV/nucleon are presented as histograms in Fig. 7(a) and (b). The solid curves in each frame are the Gaussian fits to the 19.7 MeV/nucleon spectrum at 7° , normalized to the data in each case. Figure 7(c) shows the 30 MeV/nucleon spectrum shifted in energy by a factor of $\sqrt{19.7/30}$. This direct comparison favors the conclusion that excitation is really independent of the bombarding energy. This conclusion can be made more quantitative if one deduces the χ^2 between the data and curves in parts (b) and (c); the χ^2 is a factor of ~ 2 larger in part (c) than in part (b). The lack of dependence on the incident energy indicates

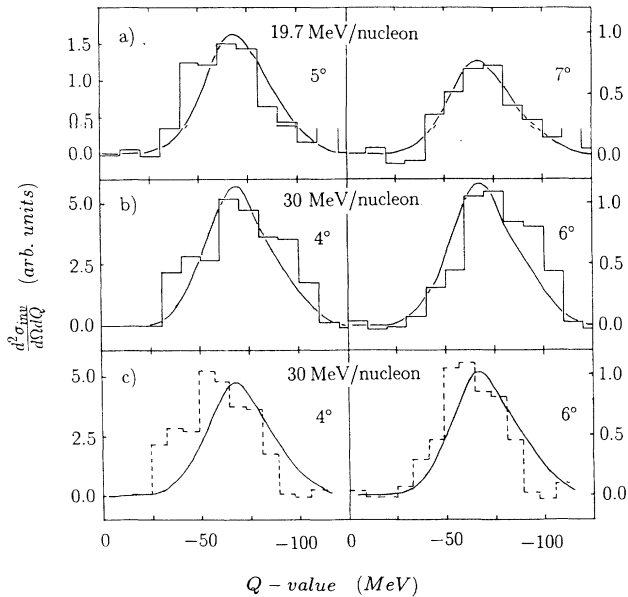


FIG. 7. Observed enhancements in the Q spectra at two forward angles and two bombarding energies [histograms in parts (a) and (b)]. The solid lines represent the shape of the spectrum at 19.7 MeV/nucleon and 7° obtained by fitting to three Gaussians. In part (c) the dashed-line histograms show the 30 MeV/nucleon spectra shifted by a factor of $\sqrt{19.7/30}$ (see text).

that the origin of the excitation lies not in the reaction dynamics but rather in the nuclear structure.

The experimental angular distributions of the mutual excitation, arbitrarily normalized, are shown as points in Fig. 8. For reasons explained in Sec. III it is difficult to give absolute values of the cross sections. However, one can make a rough estimate based on an analysis of the velocity spectra for $Z = 12$, in which the observed enhancement is most prominent. This yields a value of about 300 mb/sr at 5° and 4° for the two bombarding energies, respectively.

A strong mutual excitation of low lying states in light symmetric systems comparable with single excitation was observed at lower bombarding energies (e.g., $^{28}\text{Si} + ^{28}\text{Si}$ at 3–5 MeV/nucleon [12] or $^{12}\text{C} + ^{12}\text{C}$ at 6–10 MeV/nucleon [13]). Mutual excitation observed in the present experiment involves much higher excitation energies. It obviously dominates over corresponding single excitation of projectile or target. The complicated nature of the heavy ion interaction at bombarding energies comparable with the Fermi energy makes a realistic estimation of the mutual excitation probability difficult. We decided to investigate the likelihood of mutual excitation to energies of a few tens MeV within a mean field approach offered by the distorted wave Born approximation (DWBA) method. If the double excitation probability in this model is high then, when accounting for

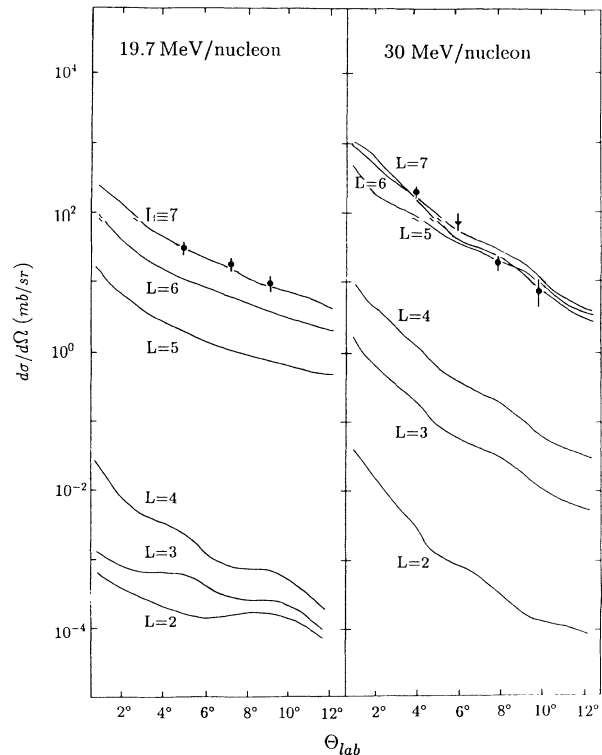


FIG. 8. Angular distribution of the observed enhancement in the Q spectra (full points) and the DWBA calculations of the mutual projectile and target excitations. The experimental angular distributions are arbitrarily normalized.

the huge enhancement due to nucleon-nucleon collisions in the overlap region of the interacting nuclei [14], the observed dominance of the mutual excitation at high excitations would be established. The results of the DWBA calculations are shown in Fig. 8 as solid lines and the details are discussed in the next section.

V. DWBA CALCULATIONS

It must be stressed that the application of the DWBA method for the present case needs to be treated with great caution and only as a very schematic approach for a few reasons. (1) At our bombarding energies the DWBA method is strictly applicable only at relatively small energy transfers (small overlap of interacting nuclei). (2) Experimental information about the Si+Si optical potential at high energies is lacking. (3) Mutual excitation implies strong coupling between reaction channels in which case a coupled channel approach is appropriate. However, for the reasons mentioned above, elaborated and computer-time-consuming coupled-channel calculations seem to be in this situation exaggerated. One has to be aware that the presented simpler DWBA calculations can provide only a guide, showing in general how feasible the mutual excitation process in studied reaction could be but of course they cannot attempt to describe the data.

Elastic and inelastic form factors used in the DWBA calculations were obtained by folding a nucleon-nucleon force with appropriate projectile and target densities [15, 16]. The real part of the Si+Si optical potential was generated by double folding of the ground-state projectile and target density distributions taken from electron scattering ($\langle r^2 \rangle^{1/2} = 3.15$ fm, $R_0 = 3.14$ fm, $a = 0.537$ fm [17]) with a central Gaussian force having a range of 1.7 fm and a volume integral of 446 MeV fm³ [18]. Such folded potentials are unphysically deep in the central region (see Fig. 9), but in the surface region which gives the main contribution to heavy ion reaction cross sections, they yield values compatible with the systematics of the experimental data (~ -100 MeV at the distance equal to the sum of the Si projectile and target radii [19]). This is shown in Fig. 9 where the solid line rep-

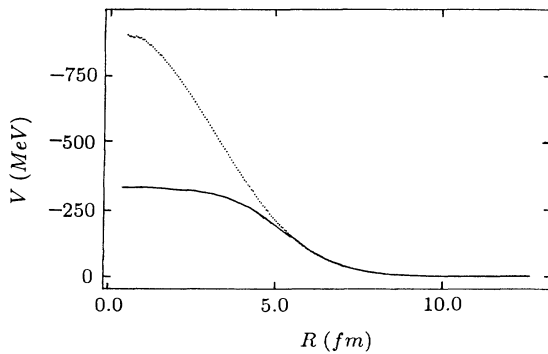


FIG. 9. Real part of the Si+Si optical potential obtained by the folding method (dotted line, see text) and a Woods-Saxon fit to the peripheral part of the potential (solid line).

resents a Woods-Saxon approximation of the folded potential at distances between projectile and target centers larger than 5.5 fm, yielding values of $V_0 = -344$ MeV, $R_0 = 0.85(A_p^{1/3} + A_t^{1/3})$ fm = 5.19 fm, and $a = 0.88$ fm.

The imaginary part of the optical potential was assumed to be of the Woods-Saxon shape with the depth -50 MeV, radius R_0 equal to the strong absorption radius of Glas and Mosel [20], $R_{SA} = 1.0(A_p^{1/3} + A_t^{1/3}) = 6.0$ fm, and the diffuseness equal to 0.54 fm. Shallow (-20 to -40 MeV) as well as deep (-40 to -60 MeV) imaginary potentials were used to describe elastic scattering of ^{12}C , ^{16}O , and ^{18}O ions from ^{28}Si nuclei at bombarding energies of 5–20 MeV/nucleon [21–24]. Our choice was motivated by the fact that at higher bombarding energies the imaginary part of the potential tends to be deeper [13].

The inelastic form factor is given by [25]

$$F(R) = (4\pi)^2 V_0 \int \int \rho_{L_p}(D, R) \rho_t(r_t) g_{L_t}(D, r_t) \times r_t^2 dr_t D^2 dD, \quad (5)$$

where $\mathbf{D} = \mathbf{R} + \mathbf{r}_p$, \mathbf{R} is the vector describing position of the projectile center in the target frame; \mathbf{r}_p and \mathbf{r}_t are vectors running over projectile and target density distributions, respectively. The function g_{L_t} comes from the multipole expansion of the nucleon-nucleon interaction:

$$V(|\mathbf{D} - \mathbf{r}_t|) = 4\pi V_0 \sum_{LM} g_{L_t}(D, r_t) Y_{LM}^*(\Omega_t) Y_{LM}(\Omega_p), \quad (6)$$

$$V_0 g_{L_t}(D, r_t) = \frac{1}{2} \int_{-1}^1 V(|\mathbf{D} - \mathbf{r}_t|) \times P_{L_t}(\cos \theta_{D, r_t}) d \cos \theta_{D, r_t}, \quad (7)$$

$$\rho_{L_p}(D, R) = \frac{1}{2} \int_{-1}^1 \rho_p(r_p) P_{L_p}(\cos \theta_{D, R}) d \cos \theta_{D, R}. \quad (8)$$

For the L_t -multipole target excitation the transition density $\rho_t(r_t)$ in Eq. (5) was assumed to have the form of the derivative of the ground state density distribution with the amplitude β given by the appropriate energy-weighted sum rule (EWSR) [26]:

$$(\hbar\omega_{L_t}) \beta_{L_t}^2 = \frac{\hbar^2}{2mR_{ss}^2} \frac{4\pi}{3A} L_t(2L_t + 1), \quad (9)$$

where the equivalent sharp radius R_{ss} is determined by the ground-state density distribution [27]:

$$\frac{1}{R_{ss}} = \frac{1}{R_0} \left[1 - \frac{7}{6} \pi^2 \left(\frac{a}{R_0} \right)^2 \right]. \quad (10)$$

In the case of a single target excitation, ρ_p is the projectile ground-state density distribution ($L_p = 0$), whereas for a double projectile and target excitation $\rho_p(r_p)$ becomes the transition density, which was taken to be exactly the same as the target transition density with $L_p = L_t = L$. Because of the possibility of different couplings between the excited projectile and the excited

target spins, the angular momentum transfer in the scattering can acquire values between $0\hbar$ and $2L\hbar$. The total mutual inelastic cross section is then

$$\frac{d\sigma_L}{d\Omega} = \sum_{L_{tr}=0}^{2L} (2L_{tr} + 1) \frac{d\sigma_{L_{tr},L}}{d\Omega}, \quad (11)$$

where the summation runs over even L_{tr} values. Calculations using the program DWUCK [28] were done for L values between 2 and 7 (the upper limit in L was determined by limitation of the angular momentum transfer in the DWUCK program to 15).

Inelastic form factors were generated using the same Gaussian nucleon-nucleon interaction as in calculations of the optical potentials. As an example, Fig. 10 displays the inelastic form factors for $L = 5$ single and mutual excitations. Above the strong absorption radius (6 fm) both form factors are similar in shape and differ only by a factor of 2–4 in magnitude.

The ratios of the mutual excitation EWSR cross sections at the Q value of -68 MeV and the single excitation EWSR cross sections at $Q = -34$ MeV for given L values are shown as a function of the laboratory angle in Fig. 11. The striking feature is an enormous enhancement of the mutual excitation at the highest L values, where the ratios are approaching a value close to 1.0. One of the reasons for this enhancement is the linear dependence of the EWSR deformation parameter β on L [see Eq. (9)], which makes ratios of the cross sections roughly proportional to L^2 . However, a more decisive

factor is the matching condition. In a classical approach the angular momentum transfer is connected with the reaction Q value through a relation:

$$L_{tr} \approx -\sqrt{\frac{\mu c^2}{2}} \frac{QR}{\hbar c \sqrt{E_{c.m.} - V_C}}, \quad (12)$$

where $E_{c.m.}$ is the initial center-of-mass kinetic energy, V_C is the Coulomb potential at the interaction radius R , and μ is the reduced mass. For the $^{28}\text{Si} + ^{28}\text{Si}$ reaction at $Q = -34$ MeV this gives $L_{tr} \approx 6$ and 5 at energies 19.7 and 30 MeV/nucleon, respectively. This matching condition, reproduced in the DWBA calculation, is demonstrated in Fig. 12, where the total inelastic cross section for the $L = 5$ single excitation divided by the cross section for $L = 0$ (calculated using the same form factor as in the $L = 5$ case; in this way the trivial dependence of the cross section on the Q value is eliminated) is shown as a function of the Q variable. The enhancement, three orders in magnitude, is well localized near $Q = -40$ MeV. For mutual excitation an additional strong enhancement is associated with the larger phase space for higher L_{tr} values. This effect is shown in Fig. 13 where the enhancement of the total mutual $L = 7$ inelastic cross section is plotted versus L_{tr} . For $Q = -34$ MeV (dashed line) L_{tr} peaks near 8 and gradually decreases above this. For $Q = -68$ MeV (solid line), however, the matching L_{tr} is roughly twice as large as in the case of $Q = -34$ MeV, resulting at $L_{tr} = 14$ in an enormous factor of 10^6 enhancement compared to $L_{tr} = 0$. This

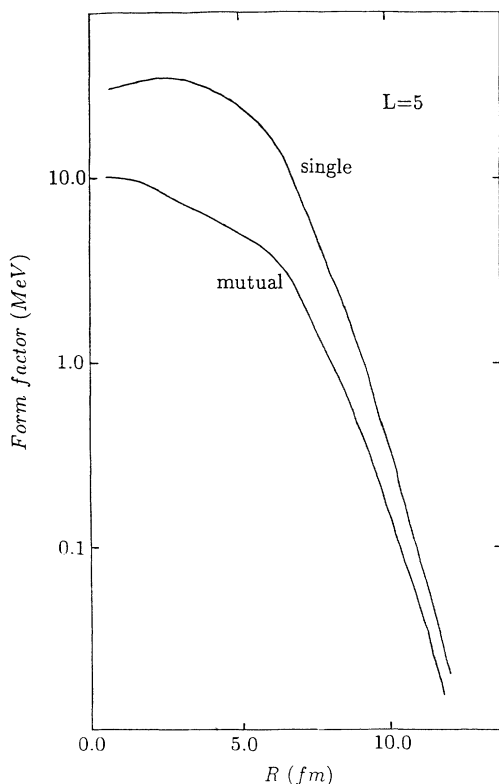


FIG. 10. Single and mutual excitation form factors for $L = 5$.

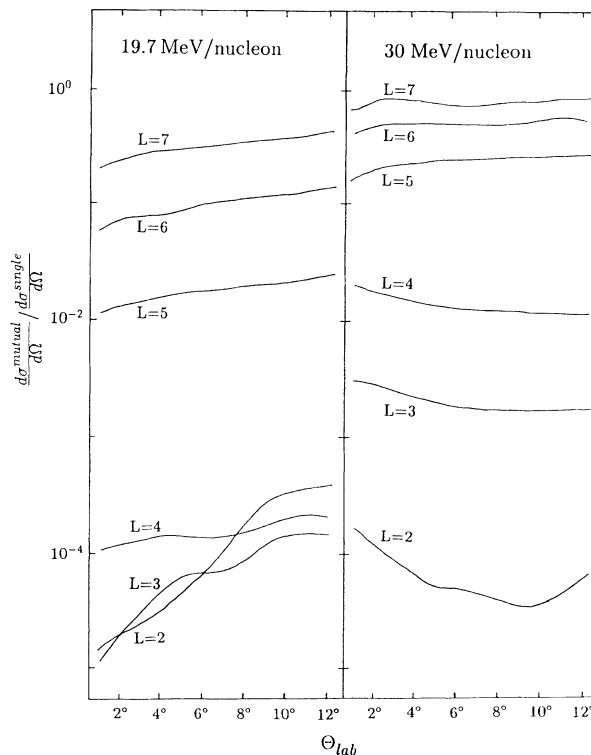


FIG. 11. Ratios of the mutual excitation inelastic cross sections to the single excitation cross sections as a function of θ_{lab} calculated within the DWBA approach.

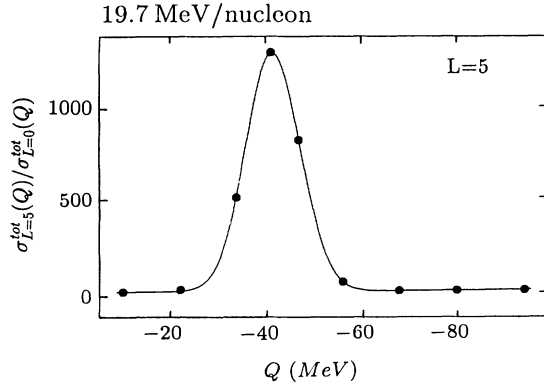


FIG. 12. Ratios of the total inelastic cross section for $L = 5$ excitation to the $L = 0$ excitation versus Q value calculated with the $L = 5$ form factor at bombarding energy of 19.7 MeV/nucleon. The solid line is a Gaussian fit with amplitude 1279, centroid -41.57 MeV and width 5.66 MeV.

strong enhancement corresponds to the classical picture in which two interacting spheres acquire parallel angular momenta. The mutual excitation enhancement should be the most pronounced in symmetric systems because in asymmetric cases the angular momentum is transferred mainly to one, heavier (larger) partner, which means that the matching condition is not necessarily fulfilled (one expects a favorable excitation energy to be larger in the lighter partner than in the heavier partner).

The slopes of the calculated mutual excitation angular distributions shown in Fig. 8 match well with the slopes of the experimental angular distributions. They are determined mainly by a reaction kinematics, so it is not surprising that DWBA calculations, being in our case a very crude approximation, are able to reproduce them. However, the calculations show that even in the DWBA approach the probability of a mutual projectile and target excitation to energies of a few tens MeV can reach values comparable with the probabilities of a single excitation. In a grazing interaction at high bombarding energy the nucleon-nucleon collisions will significantly enhance this probability further [14].

VI. CONCLUSIONS

The results presented above show that in the symmetric $^{28}\text{Si} + ^{28}\text{Si}$ system the selective mutual excitation of the projectile and target to the energies of 30–40 MeV is a dominant process which must play an important role in energy dissipation in the initial stages of peripheral reactions. The favorable angular momentum transfer matching such excitations is $(5-6)\hbar$. The enhancement of the mutual excitation at high excitation energies and high spins is reproduced even in mean-field DWBA calculations.

The observed most favorable energies fall in the region

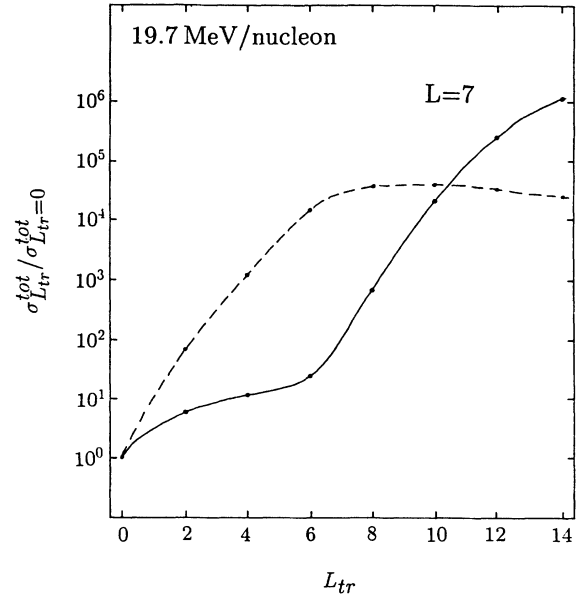


FIG. 13. Total mutual $L = 7$ inelastic excitation cross sections at 19.7 MeV/nucleon versus different angular momentum transfers. The solid line presents calculations at $Q = -68$ MeV and the dashed line at $Q = -34$ MeV. To eliminate the trivial Q dependence, the cross sections were divided by the cross sections for $L_{tr} = 0$.

of $(2-3)\hbar\omega$ excitations. At these energies a nucleus is much less “rigid” and in a violent collision might easily undergo giant (collective) oscillations. On the other hand, the selectivity in the excitation energy may be caused by an incoherent bidirectional nucleon transfer from occupied states in one reaction partner to the empty shell of the other [29]. This selective excitation of either coherent or incoherent nature, which must occur at a very early stage of the reaction (the cross section is the largest at very forward angles), provides an important doorway to other dissipative processes. This effect should be a common feature in reactions involving various symmetric systems at different bombarding energies. They should also exhibit a similar pattern of excitation since the matching angular momentum [Eq. (12)] depends weakly on the bombarding energy ($E_{c.m.}^{-1/2}$) and does not depend on the system ($QR \approx \text{const}$ if $Q \sim -\hbar\omega$).

ACKNOWLEDGMENTS

We would like to thank the staff of SARA for providing us with the Si beams. This work was part of the research program of the “Stichting voor Fundamenteel Onderzoek der Materie” (FOM), with financial support from the “Nederlandse Organisatie voor Wetenschappelijk Onderzoek” (NWO).

- [1] R.A. Broglia, C.H. Dasso, and A. Winther, *Phys. Lett.* **61B**, 113 (1976).
- [2] Ph. Chomaz, Y. Blumenfeld, N. Frascaria, J.P. Garron, J.C. Jacmart, W. Bohne, A. Gamp, W. Von Oertzen, Nguyen Van Giai, and D. Vautherin, *Z. Phys. A* **319**, 167 (1984); Ph. Chomaz, Nguyen Van Giai, and D. Vautherin, *Nucl. Phys.* **A476**, 125 (1988).
- [3] E. Suraud, M. Pi, and P. Schuck, *Nucl. Phys.* **A482**, 187c (1988); E. Suraud, M. Pi, P. Schuck, B. Remaud, F. Sebillie, C. Gregoire, and F. Saint-Laurent, *Phys. Lett. B* **229**, 359 (1989).
- [4] R.J. Meijer, G.J. van Nieuwenhuizen, A. van den Brink, P. Decowski, K.A. Griffioen, and R. Kamermans, *Nucl. Instrum. Methods* **A264**, 285 (1988).
- [5] R.J. Meijer, A.P. de Haas, J.J. Langerak, C.J. Oskamp, W. Smit, M. Voerman, P. Decowski, K.A. Griffioen, G.J. van Nieuwenhuizen, and R. Kamermans, *Nucl. Instrum. Methods* **A265**, 511 (1988).
- [6] R.J. Meijer, P.F. Box, P. Decowski, E. Gierlik, R. Kamermans, G.J. van Nieuwenhuizen, K.A. Griffioen, H.W. Wilschut, A. Giorni, C. Morand, A. Demeyer, and D. Guinet, *Phys. Rev. C* **44**, 2625 (1991).
- [7] P.J. Siemens, J.P. Bondorf, D.H.E. Gross, and F. Dickmann, *Phys. Lett.* **36B**, 24 (1971); Y. Alhassid, R.D. Levine, J.S. Karp, and S.G. Steadman, *Phys. Rev. C* **20**, 1789 (1979); J. Wilczyński, in *Proceedings of the International Conference on Nuclear Physics, Florence, 1983*, edited by P. Blasi and R.A. Ricci (North Holland, Amsterdam, 1984), Vol. II, p. 305.
- [8] S.B. Gazes, H.R. Schmidt, Y. Chan, E. Chavez, R. Kamermans, and R.G. Stokstad, *Phys. Rev. C* **38**, 712 (1988).
- [9] J. Wilczyński and H.W. Wilschut, *Phys. Rev. C* **39**, 2475 (1989).
- [10] F. Pühlhofer, *Nucl. Phys.* **A280**, 267 (1977).
- [11] K. Siwek-Wilczyńska, R.A. Blue, L.H. Harwood, R.M. Ronningen, H. Utsunomiya, J. Wilczyński, and D.J. Morrissey, *Phys. Rev. C* **32**, 1450 (1985); J. Wilczyński, J.D. Hinnefeld, E.E. Koldenhof, H.K.W. Leegte, R.H. Siemssen, H.W. Wilschut, and Y.X. Xie, *Phys. Lett. B* **220**, 497 (1989).
- [12] R.R. Betts, H.-G. Clerc, B.B. Back, I. Ahmad, K.L. Wolf, and B.G. Glagola, *Phys. Rev. Lett.* **46**, 313 (1981).
- [13] R.G. Stokstad, R.M. Wieland, G.R. Satchler, C.B. Fulmer, D.C. Hensley, S. Raman, L.D. Rickertsen, A.H. Snell, and P.H. Stelson, *Phys. Rev. C* **20**, 655 (1979).
- [14] J. Aichelin and H. Stöcker, *Phys. Lett.* **163B**, 59 (1985).
- [15] G.R. Satchler, *Direct Nuclear Reactions* (Oxford University Press, New York, 1983).
- [16] G.R. Satchler and W.G. Love, *Phys. Rep.* **55**, 183 (1979).
- [17] C.W. De Jager, H. de Vries, and C. de Vries, *At. Data Nucl. Data Tables* **14**, 479 (1974).
- [18] H.P. Morsch, P. Decowski, and W. Benenson, *Nucl. Phys.* **A297**, 317 (1978).
- [19] G.R. Satchler, *Nucl. Phys.* **A409**, 3c (1983).
- [20] D. Glas and U. Mosel, *Nucl. Phys.* **A237**, 429 (1975).
- [21] T. Yamaga, O. Satoh, M. Morita, K. Kotajima, K. Hasengawa, T. Shinozuka, and M. Fujioka, *Phys. Rev. C* **37**, 2585 (1988).
- [22] M.A.G. Fernandes, B.L. Burks, D.J. Horen, G.R. Satchler, R.L. Auble, F.E. Bertand, J.L. Blankenship, J.L.C. Ford, E.E. Gross, D.C. Hensley, R.O. Sayer, D. Shapira, and T.P. Sjoneen, *Phys. Rev. C* **33**, 1971 (1986).
- [23] R.M. DeVries, D.A. Goldberg, J.W. Watson, M.S. Zisman, and J.G. Cramer, *Phys. Rev. Lett.* **39**, 450 (1977).
- [24] J.G. Cramer, R.M. DeVries, D.A. Goldberg, M.S. Zisman, and C.F. Maguire, *Phys. Rev. C* **14**, 2158 (1976).
- [25] R. Kamermans, H.P. Morsch, R.J. de Meijer, and J. van Driel, *Nucl. Phys.* **A314**, 37 (1979).
- [26] E.C. Halbert, J.B. McGrory, G.R. Satchler, and J. Speth, *Nucl. Phys.* **A245**, 189 (1975).
- [27] A. Bohr and B.R. Mottelson, *Nuclear Structure* (Benjamin, New York, 1969), Vol. 1.
- [28] P.D. Kunz, computer program DWUCK (unpublished).
- [29] K. Werner, *Nucl. Phys.* **A453**, 486 (1986).